nzsee
NEW ZEALAND SOCIETY FOR EARTHQUAKE ENGINEERING

Design of RSFJ self-centring brace for ultimate limit state

S.M.M. Yousef-beik & P. Zarnani

Auckland University of Technology, New Zealand.

S. Varier

Tectonus Ltd, Auckland.

A. Hashemi & P. Quenneville

University of Auckland, New Zealand, Auckland.

ABSTRACT

In previous studies, it was shown that the RSFJ brace assembly is prone to elastic buckling for which a new mechanism composed of two telescopic sections was introduced as a remedy to increase the elastic buckling load, and it was named as "Anti-buckling tubes" (ABT). However, designing the RSFJ brace for the elastic buckling may not be conservative, though strengthened with ABT, mainly because some part(s) of the brace may fail due to second-order actions (mainly moment) before hitting the elastic buckling. Therefore, in the present study, the inelastic buckling of the RSFJ brace assembly is going to be discussed, which is supposed to be the ultimate strength of the brace in compression. For this, a simplified closed-form formulation is developed which an engineer can simply employ to quantify and approximate that ultimate strength. The suggested framework is validated with a number of numerical examples using ABAQUS finite element software. Apart from those, some seismic design consideration will be discussed in order to guarantee that the brace will perform as it is expected at the time of the seismic event. Finally, and in the interest of further clarification, an example of a brace design procedure for a real case is provided.

1 INTRODUCTION AND BACKGROUND

The resilient slip friction joint (RSFJ) is a relatively new self-centring friction damper that dissipates the input energy through a passive damping and a slip-friction mechanism (Zarnani and Quenneville 2015), which can be applied in different lateral load resisting systems. Among several applications, it can be referred to the self-centring tension-compression braces (Hashemi, Yousef-Beik et al. 2019, Yousef-beik, Bagheri et al. 2020, Yousef-beik, Veismoradi et al. 2020, Yousef-beik, Veismoradi et al. 2020), self-centring tension-only braces (Bagheri, Hashemi et al. 2020, Bagheri, Hashemi et al. 2020), rocking timber or concrete shear walls (Darani, Zarnani et al. 2018, Hashemi, Bagheri et al. 2020), rocking steel braced frames with shear links (Sahami, Zarnani et al. 2020) and MRFs (Shabankareh, Veismoradi et al. 2020) and rotational links (Veismoradi, Zarnani et al. 2019).

RSFJ brace assembly is a self-centring brace that is composed of three main elements as depicted in Fig.1. The first element is the damper, which depending on the displacement demand can be located in either one or two locations along with the brace. The second element is the brace body, which depending on the architectural or structural considerations can be made up of either timber or steel. The last but not the least element is the telescopic steel tubes entitled "Anti-Buckling Tubes or ABT", which are responsible to strengthen the brace where dampers are located, thereby increasing the compressive elastic buckling capacity of the brace. Previous studies (Hashemi, Yousef-Beik et al. 2019, Yousef-beik, Zarnani et al. 2019, Veismoradi, Quenneville et al. 2020, Yousef-beik, Bagheri et al. 2020, Yousef-beik, Veismoradi et al. 2020, Yousef-beik, Veismoradi et al. 2020) demonstrated that if the RSFJ brace is not equipped with the ABTs, the compression capacity of the brace would be very low because of the rotational flexibility of RSFJ. To strengthen the brace against premature instability, the telescopic ABTs are installed in parallel to the damper(s) to increase their rotational stiffness. The closed-form equation to calculate the elastic buckling of the strengthened brace with ABT was proposed in the previous study (Yousef-beik, Veismoradi et al. 2020). In this regard, it will be shown that even if the elastic buckling capacity of the brace is improved with ABTs, this load cannot be a reliable indicator for the design. In fact, the ultimate capacity of the brace in compression might be lower than that improved elastic buckling capacity due to arrival of second-order actions. This paper first deals with establishing a proper framework for the design of the RSFJ brace for ultimate strength in compression, then validate it with numerical analysis. Finally, an example brace design with complementary seismic design considerations will be provided for better clarification and illustration.

2 ULTIMATE STRENGTH QUANTIFICATION

Compressive behaviour of any steel members can be categorized in one of the behaviours described in Fig.2 (Bažant and Cedolin 2010). The curve with the black line is the real performance of the member when tested in the laboratory. The purple line is the Euler load -"P_E"- to which the blue dotted curve will asymptotically approach. This curve shows the effect of P-δ and intial imperfection. Finally, the red dotted line shows the combined action diagram which shows the strength will decrease from the maximum of section capacity "P_n" with the increase in lateral displacement of the member. As evident from Fig.2, the ultimate strength of the member can be approximated with the intersection point (red circle) between the stiffness deterioration curve (known as $P-\delta$ path) and the strength deterioration curve (known as *combined action* path).

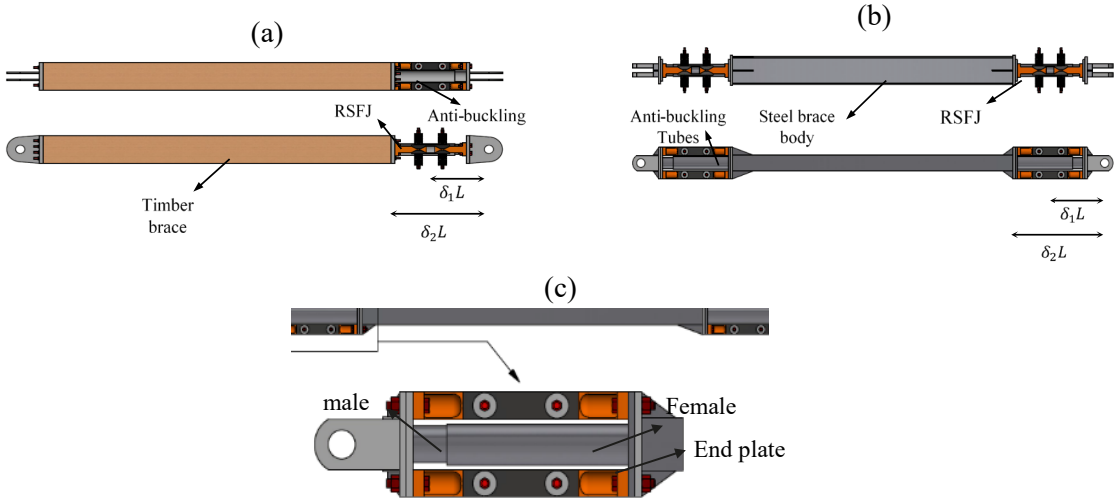

Figure 1: (a) RSFJ brace with one damper and timber brace body, (b) RSFJ brace with two dampers and steel body and (c) proposed arrangment for female and male sections

In the first case shown in Fig.2.a, if the axial section-capacity -"P_n" -is less than then Euler buckling load "P_E" (stocky members or members having low slenderness ratio), the ultimate strength of the member is less than both of the section-capacity and the Euler load. Moreover, the plastic hinge tends to be formed at a relatively small amount of lateral displacement "δ". In contrast to this case is the second case described in Fig.2.b. If the section-capacity "P_n" is higher than the Euler buckling load "P_E" (slender members or members having high slenderness ratio), the ultimate strength of the member would be almost equal to the Euler load "P_E", and at a relatively large lateral displacement "δ", the plastic hinge will form at the critical section.

From the stability of structures (Bažant and Cedolin 2010), the stiffness deterioration curve is known as:

$$P(\delta) = P_E \frac{\delta}{\delta+\delta_0} \tag{1}$$

in which the Euler buckling load for the RSFJ brace assembly can be calculated as (Yousef-beik, Veismoradi et al. 2020)

$$P_E = \alpha \frac{EI}{L^2} \tag{2}$$

where parameter α is derived from the following equation as the minimum real root (Yousef-beik, Veismoradi et al. 2020) and it is bounded between zero and π^2:

$$f(\delta_1,\beta) = \beta\, tan(\delta_1\sqrt{\alpha}) - tan\left(\sqrt{\alpha}\,(1-\delta_1)\right)\left[\sqrt{\alpha}\, tan(\delta_1\sqrt{\alpha}) - \beta\right] \tag{3}$$

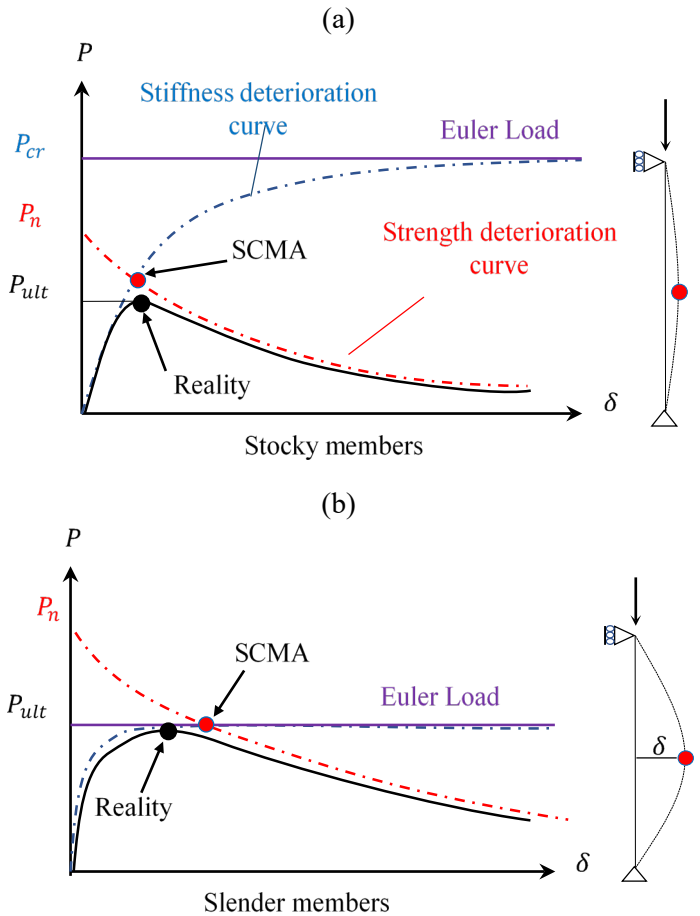

Figure 2: Compressive behaviour of steel columns (Bažant and Cedolin 2010): (a) stocky members and (b) slender members

Relative location and rotational stiffness of the non-continuity region (Fig.1) is represented by the parameters "δ_1" and "β", respectively and can be calculated using Eq.4 and Eq.5:

$$\delta_1 = \frac{0.5L_{RSFJ}+L_{con}}{L} \tag{4}$$

$$\beta = \frac{(K_{rot})_{ABT}L}{EI} \tag{5}$$

in which $(K_{rot})_{ABT}$ is the rotational stiffness of the non-continuity region, which is assumed to be only reliant on Anti-buckling tubes (ABTs). This parameter can be simply derived using the method of virtual work (Hibbeler and Kiang 2015). The rotational stiffness of the ABTs is illustrated in Eq.6:

$$(K_{rot})_{ABT} = \frac{2m.EI_{ABT}}{\delta_2 L} \tag{6}$$

in which

$$m = \frac{\delta_2}{[2(\delta_2-\delta_1)-(\delta_2)^2+\beta_b(1-\delta_2)^2]} \tag{7}$$

when the elastic buckling load (Euler load) is determined, the stiffness deterioration curve can be approximated using Eq.1 in which the initial imperfection is:

$$\delta_0 = \frac{L}{1000} + \frac{L}{500} + \delta_{clearance} \tag{8}$$

in which the initial imperfection of the body is (L/1000), erection tolerance is L/500 and clearance in the gusset and/or ABTs is $\delta_{clearance}$. In the two above mentioned equations, parameters β_b and δ_2 are the relative rigidity and relative length of ABT:

$$\beta_b = \frac{EI_{ABT}}{EI} \tag{9}$$

$$\delta_2 = \frac{L_{RSFJ}+L_{con}}{L} \tag{10}$$

The strength deterioration path can be simply derived from the collapse mechanism (plastic analysis) as below:

$$P = \frac{M_p}{\delta} \tag{11}$$

in which "M_p" is the plastic capacity of the critical section. Note that this plastic hinge moment capacity should be modified and reduced if there is an axial load. It should be noted that there might be a number of critical sections for the RSFJ brace assembly. In that case, a number of ultimate loads can be approximated based on the intersection of stiffness deterioration curve and the different strength deterioration curves. The lowest force obtained from the results shall be considered as the system ultimate capacity. More clarification is provided in the next section.

3 VALIDATION WITH NUMERICAL STUDY

For the purpose of numerical finite element study, six types of telescopic circular hollow sections were employed in the role of ABTs. These sections were assumed to be made up of the mild steel with the elastic modulus of 200 GPa, yield strength of 340 MPa and ultimate strain of 0.2. These sections are tabulated in Table.1. Furthermore, the brace body was assumed to be of steel type in which one location was considered for installation of the damper(s), and it had box cross-section with a width of 152.5 mm and thickness of 9.5 mm. Further information regarding the geometry is provided in Table.1.

Table. 1: ABT info for numerical models

Scenario	ABT type	$(D_{out})_f$ (mm)	$(D_{in})_f$ (mm)	$(D_{out})_m$ (mm)	$(D_{in})_m$ (mm)	$\delta_2 L$ (mm)	$\delta_1 L$ (mm)	L_{RSFJ} (mm)	L (mm)
1	ABT 1	100.30	89.50	88.30	77.50	835	633	633	4156
2	ABT 2	110.30	99.50	98.30	87.50				
3	ABT 3	120.30	109.50	108.30	97.50				
4	ABT 4	140.30	129.50	128.30	117.50				
5	ABT 5	80.3	69.5	68.3	57.5	400	295	210	
6	ABT 6	120.3	109.5	108.3	97.5				

The inelastic buckling analysis was performed in the ABAQUS software environment using the "Arc Length method" or "the modified Riks analysis" (Riks 1979). Fig.3 shows the model in the ABAQUS environment where the RSFJs were idealized with two rectangular plates attached together using a rotational hinge link without any moment transfer capacity. The rotational behaviour of the RSFJ was ignored as it is negligible compared to ABT. For the modelling of the different part of the brace, the 20-node 3D quadratic brick element was used so that the errors in the results are minimum. Different parts of the model were attached together using "Tie" constraint. The anti-buckling tubes were attached using a link with a released axial degree of freedom and restrained rotational degree-of-freedom.

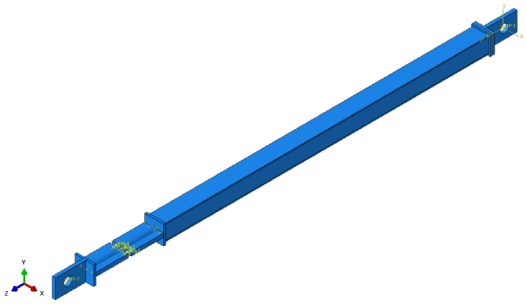

Figure 3: Finite element modeling of the RSFJ brace in ABAQUS environment

Fig.4 shows the results of ABAQUS simulation as compared to prediction with the proposed framework. In the case of RSFJ brace, two critical sections exist in terms of checking for the strength. The first one is the midspan of the brace subjected to the largest second-order moment and also axial compressive force. The second critical section is where the ABT female part is attached to the brace body (Fig.1). At this section, the ABT should be checked for the second-order moment. Note that the ABTs should not be checked for the "*combined action*" as its axial degree of freedom is released due to the telescopic instalment. As shown in Fig.4 and reported in Table.2, the proposed framework could successfully predict both failure mode, which is either midspan or ABT, and the ultimate load with acceptable accuracy for the four scenarios. This accuracy will be more discussed in the next section.

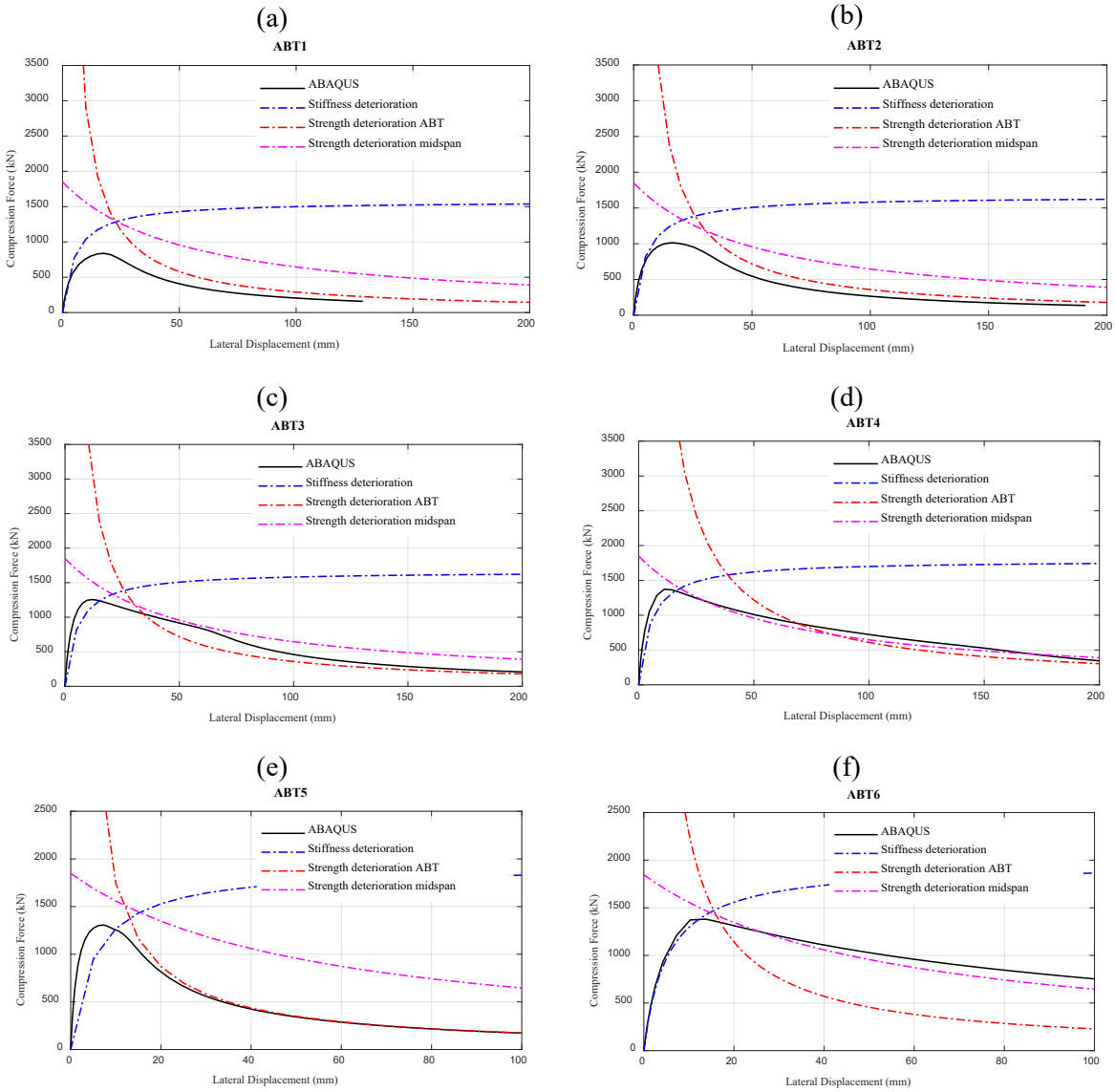

Figure 4: Numerical Vs Analytical predictions for ultimate limit state load of RSFJ brace: (a) scenario 1 – ABT failure, (b) scenario 2 – brace body failure, (c) scenario 3 – brace body failure, d) scenario 4 – brace body failure, e) scenario 5 – ABT failure and f) scenario 6 – brace body failure

4 PARAMETRIC FINITE ELEMENT STUDY

As discussed in the previous section, the methodology presented in this paper could successfully predict the ultimate load and the failure mode of the RSFJ brace assembly with acceptable accuracy. However, it was observed that the prediction of the failure load had a varying degree of difference with numerical results though it was negligible (less than 25% difference). The root cause of this difference is shown in Fig.5 and lies in the fact that the real ultimate load of the brace falls below the intersection point. More specifically, the intersection point would be always an upper limit for the ultimate load. Accordingly, this section is dedicated to quantifying a calibration factor in a way to bring down the intersection load to match the finite element (reality) load. To do so, a number of ABTs were chosen in a way that the parameter β_b varies between 0.035 and 0.9. To further investigate the effect of the damper length, three scenarios – ABT relative length (δ_2) to be 10, 20 and 25% of the brace length – were considered for the length of the damper.

Table.2: ABAQUS results Vs Analytical predictions

Scenario	ABT type	β_b	Failure mode ABAQUS	Failure mode prediction	Ultimate load ABAQUS	Ultimate Load prediction	Error %
1	ABT 1	0.16	ABT	ABT	1011	1283	26.90
2	ABT 2	0.22	Midspan body	Midspan body	1142	1332	16.64
3	ABT 3	0.3	Midspan body	Midspan body	1243	1359	9.33
4	ABT 4	0.49	Midspan body	Midspan body	1343	1386	3.20
5	ABT 5	0.077	ABT	ABT	1307	1369	4.7
6	ABT 6	0.3	Midspan body	Midspan body	1380	1462	5.9

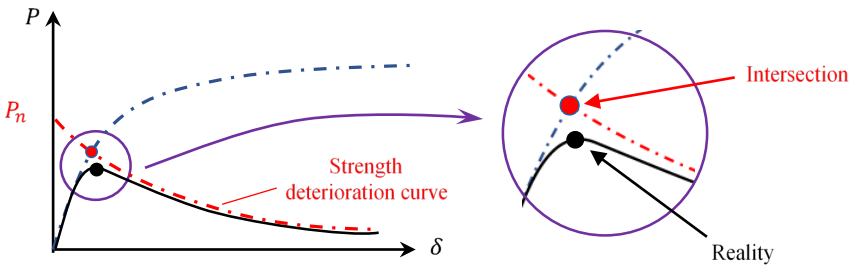

Figure 5: Real ultimate load Vs upper limit as the intersection point

Fig.6.a shows the result of finite element study and the value of calibration factor. A calibration factor of one implies that the result of analytical approach matches the numerical one. It can be observed that for all three scenarios, the calibration factor approaches one as the relative rigidity β_b increases. It can be also deduced that the shorter damper is, faster the calibration factor approaches 1.0. At the interest of safety and simplicity of design, a unit calibration factor can be assumed to different zones. For example, for the blue and the green zone, a calibration factor of 0.85 and 0.75 can be assumed, respectively. The grey zone involves a large portion of inaccuracy and also tends to be not practical for design (small amount of β_b).

If the results of the finite element study are sorted out based on the calibration factor (Eq.12), relative rigidity and length, Fig.6.b would be envisioned. As mentioned before, this diagram has been divided to three zones. These zones are formulated as a piece-wise function shown in Eq. 13.

$$P_{ult,mod} = \gamma_c P_{ult} = \gamma_c P_{cr} \frac{\delta_{int}}{\delta_{int}+\delta_0} \tag{12}$$

$$\gamma_c = \begin{cases} 0.85 & \delta_2 > 0.1 \ \ and \ \ \beta_b \geq 0.0115e^{14.54\delta_2} \\ 0.75 & \delta_2 > 0.1 \ \ and \ \ \beta_b \geq 0.0083e^{14.54\delta_2} \\ 0.85 & \delta_2 < 0.1 \ \ and \ \ \beta_b \geq 0.05 \\ 0.75 & \delta_2 < 0.1 \ \ and \ \ \beta_b \geq 0.035 \\ Not\ Practical & else \end{cases} \tag{13}$$

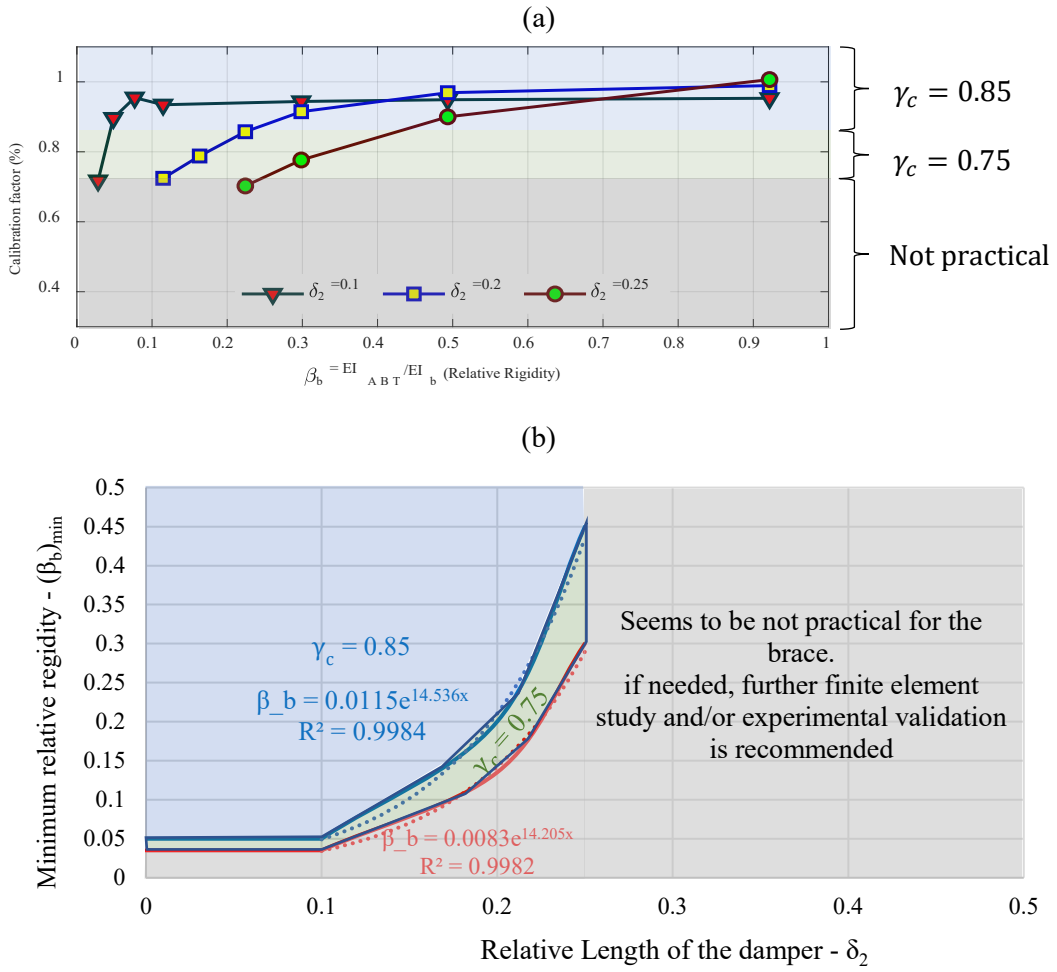

Figure 6: Calibration factor for Brace Design: (a) Calibration factor for a brace with different damper length and (b) Simplification of the calibration factor for design purposes

5 CAPACITY DESIGN CONSIDERATIONS

As discussed, two possible failure modes may exist for the RSFJ self-centring brace. The first one is that the plastic hinge forms within the damper location and in the female part of the ABT (shown in Fig.1.c). This scenario is more probable when the relative rigidity ($\beta_b = EI_{ABT}/EI_{bb}$) of the ABT to brace body is small (ABT1 in Table.2). The second scenario is that the plastic hinge forms at the mid-span of the brace and within the brace body. This is more probable when the relative rigidity (β_b) is considerable (ABT 2, 3 & 4 Table.2). The latter case is desirable and recommended to be governed in the design process mainly because if the plastic hinge forms within the ABT, it indicates that the damper is damaged, and it may not resist any further inelastic load either in the mainshock or aftershocks. However, if the plastic hinge is formed at the brace body, the whole brace can be effective almost intact in the tension cycles but with a degraded strength in the compression cycles.

Normally shear force in the braces is negligible since originating from the second-order actions, but they can be critical in some cases (designing connections, welding and so on) and discussed here accordingly. Assuming that the plastic hinge is formed at mid-span of the brace (desirable mode), the deflected shape at ultimate limit state would be:

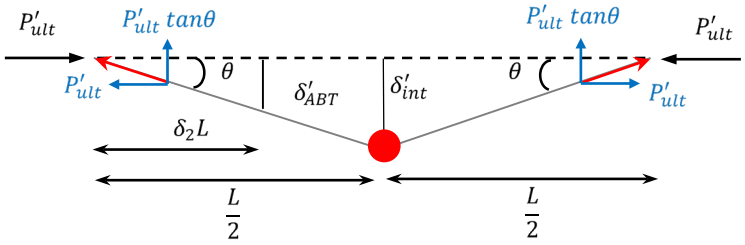

Figure 7: Expected deformed shaped at ultimate limit state

According to the Fig.7 and assuming that the deformations are of small magnitude ($sin\theta \sim tan\theta \sim \theta$ & $cos\theta \sim 1$), the shear force due to second-order action can be approximated with the vertical component of the ultimate load as "$P'_{ult}\ tan\theta$ or $P'_{ult}\ \theta$". It should be pointed out that the "P'_{ult}" and "δ'_{int}" are the amplified ultimate load and intersection point with respect to the material overstrength. In another word, the strength deterioration curve should be factored by the material overstrength, and then the new ultimate load and intersection point should be recalculated. The stiffness deterioration curve does not need to be changed as it is independent of the material yielding limit. This modification originates from the well-known capacity design concept and the fact that the adjacent members of a seismic fuse should stay elastic for the factored plastic capacity of the fuse.

If the initial imperfection (L/1000) of the body, erection tolerance (L/500) and clearance in the connection is also considered, the modified shear force can be calculated using Eq.14:

$$V_u = P'_{ult}\left(\frac{2\delta'_{int}}{L} + \frac{1}{1000} + \frac{1}{500} + \theta_{clearance}\right) \geq 0.004P'_{ult} \quad (14)$$

where $\theta_{clearance}$ is the additional initial rotation due to possible clearance in the connections (gusset plate and ABTs). The value of shear force is also recommended to be more than $0.004P'_{ult}$, suggested by the AISC 360 (AISC 2010) – Appendix 6 (requirement for column bracing). In this regard, all the elements of the brace should be checked to be able to resist this shear.

Another point that should be considered in the seismic design is the design of end plates of ABT and RSFJ as shown in Fig.1.c. This plate should possess a sufficient stiffness and strength so that the performance of the brace is not disrupted. In the first case, if the governing failure mode is the plastic hinge within the ABT, then the endplate should be designed in a way to be capable of accommodating the factored plastic capacity of the ABTs (plastic capacity including the overstrength). In the second case; however, if the governing failure mode is the plastic hinge within the brace body, then the endplate can be designed for the applied moment at the location of ABT as shown in Eq.15, which is less demanding compared to the first case:

$$\left(M_{ep}\right)^* = P'_{ult}\delta'_{ABT} \sim P'_{ult}(2\delta_2\delta'_{int}) \quad (15)$$

In terms of stiffness, requirement, the end plate should be stiff enough so that no localized rotation occurs in the plate.

6 DESIGN EXAMPLE

The objective in this section is to design a brace for 1300 kN capacity in which all of the members are made up of mild steel with elastic modulus of 200 GPa and yield stress of 340 MPa. The total length of the brace is 8460 mm while the damper length is 1310 mm and the distance between pin and damper is 200 mm. The following parameters has been assumed as the input: Overstrength factor (o/s) = 1.35, which is concerning the performance of RSFJ after lockage, referred to as secondary-fuse (Bagheri, Hashemi et al. 2020). This makes the force demand factored to P = 1.35 * 1300 = 1755 kN (Factored Force Demand). The brace section was of CHS (Circular Hollow

Section) CHS 323.9 x 9.5 with moment of inertia of 11600 e4 mm^4. The relative length of the ABT and RSFJ given that L_{RSFJ} = 1310 mm can be calculated from Eq.4 and Eq.10 as following:

$$\delta_1 = \frac{835}{8460} \sim 0.1$$

$$\delta_2 = \frac{1510}{8460} \sim 0.18$$

The anti-buckling tubes were assumed to be composed of two telescopic SHS (Square Hollow Section) with dimensions 125 mm and 107 mm for female section and 105 mm and 87 mm for female part, respectively. The moment of inertia for female and male section were 9.433 e6 and 5.366 e6 mm^4. For this design, three number of ABTs has been provided with RSFJ on either side on the RBA:

The parameter "β_b" – relative rigidity – should be calculated for both weak and strong axis (here same for CHS section) from Eq.9:

$$(\beta_b)_{weak} = \frac{200{,}000 * 3(9.433 + 5.366) * 10^6}{200{,}000 * 11600 * 10^4} = 0.38$$

$$(\beta_b)_{strong} = \frac{200{,}000 * 3(9.433 + 5.366) * 10^6}{200{,}000 * 11600 * 10^4} = 0.38$$

The parameter "m" should be calculated for both weak and strong axis from Eq.7:

$$(m)_{weak} = 0.469$$

$$(m)_{strong} = 0.469$$

The rotational stiffness of ABT "K_{ABT}" should be calculated for both weak and strong axis from Eq.6:

$$(K_{ABT})_{weak} = 5.5\text{ e9 N.mm}$$

$$(K_{ABT})_{strong} = 5.5\text{ e9 N.mm}$$

The parameter "β" – relative stiffness – should be calculated for both weak and strong axis from Eq.5:

$$(\beta)_{weak} = 2.007$$

$$(\beta)_{strong} = 2.007$$

The parameter "α" should be calculated by solving the characteristic equation (Eq.3) for both weak and strong axis for the finite minimum non-zero real roots:

$$(\alpha)_{weak} = 8.606$$

$$(\alpha)_{strong} = 8.606$$

Finally, the Euler load (elastic buckling load) "P_{cr}" should be calculated for both weak and strong axis from Eq.2:

$$(P_{cr})_{weak} = 2789.76\text{ kN}$$

$$(P_{cr})_{strong} = 2789.76\text{ kN}$$

As it is was mentioned before, this elastic buckling load is not an indicator of the system capacity in compression.

Calculation of the possible clearances and imperfections:

- ✓ $L/500$ for the total out-of-straightness of the brace and erection error
- ✓ Clearance between male and female telescopic tubes as per Table.3

$\delta_0 = \frac{8460}{500} + 2 = 18.9\ mm$

Strength curves associated with ABT (female) and the brace body can be derived from Eq.11:

$$P_{ABT}(\delta) = \frac{(M_p)_f}{\delta}$$

$$P_{body}(\delta) = \frac{(M_p)_{body}\left(1 - \frac{P_{body}}{P_n}\right)}{\delta}$$

or

$$P_{body} = \frac{(M_p)_{body}}{\frac{(M_p)_{body}}{P_n} + \delta}$$

Note that the strength of the brace body is modified with combined action formula given it is carrying axial load and bending moment at the same time. However, the ABT does not need modification as it is not carrying any axial load.

Plastic modulus of female part of ABT = number of ABT × $\left(\frac{bh^2}{4} - (b-2t)(\frac{h}{2}-t)^2\right)$

$S_{ABT} = 1.82$ e5 mm3

Plastic moment capacity of ABT and brace body

$(M_p)_{female} = S_{female} \times F_y = 185.66$ kNm

$(M_p)_{body} = S_{body} \times F_y = 319.26$ kNm

Nominal axial capacity of brace body (Squash load): $P_n = A_g F_y = 3189.20$ kN

The intersection points can be approximated using the following equations and shown in Fig.8:

$$(\delta_{int})_{ABT} = 0.5(M_p)_{female}\left[\frac{1}{P_E} + \sqrt{\left(\frac{1}{P_E}\right)^2 + \frac{4\delta_0}{(M_p)_{female}.P_{cr}}}\right] = 82\ mm \quad (16)$$

$$(\delta_{int})_{body} = 0.5(M_p)_{body}\left[\frac{1}{P_E} - \frac{1}{P_n} + \sqrt{\left(\frac{1}{P_E} - \frac{1}{P_n}\right)^2 + \frac{4\delta_0}{(M_p)_{female}.P_{cr}}}\right] = 54\ mm \quad (17)$$

Finally, the ultimate load capacity of brace can be derived from Eq.1 or Eq.11 if the intersection point is assumed as the input (Fig.8).

$P_{ult} = \min\left[P_{cr} * \frac{(\delta_{int})_{ABT}}{(\delta_{int})_{ABT}+\delta_0},\ P_{cr} * \frac{(\delta_{int})_{body}}{(\delta_{int})_{body}+\delta_0}\right] = \min\left[2266,\ 2116\ kN\right] = 2116$ kN

Given that $\delta_2 = 0.18$ and $\beta_b = 0.38$, the calibration coefficient is 0.85 (Eq.13). The modified capacity of the brace can be derived from Eq.12 as:

$P_{ult,mod} = \gamma_c P_{ult} = 0.85 * 2116 = 1798.6$ kN

As it can be observed, the governing failure mode is the plastic hinge in the brace body, which was discussed to be the desired mode of failure. The next step would be the design of the endplate of the ABT, which is similar to the design of base plates. Since the governing failure mode is the plastic hinge in the brace body, the endplate can be design for the bending demand at the end of ABT at the time of plastic hinge formation (Eq.15 and Fig.7)

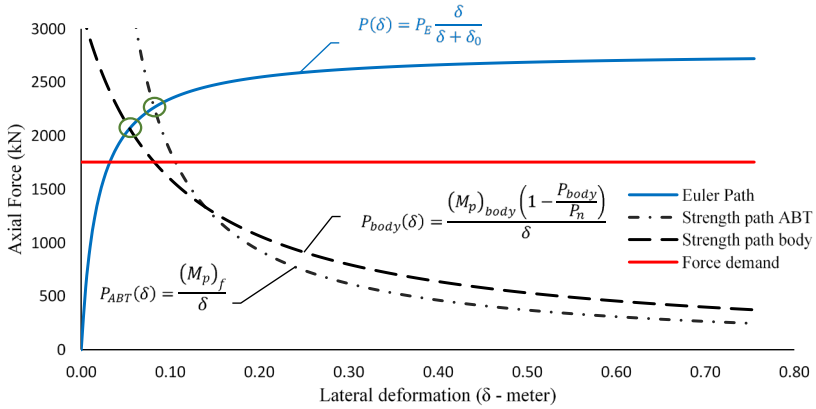

Figure 8: Spotting the ultimate capacity by intersecting the stiffness and strength deterioration curves.

Bending moment and axial force demands for endplate would be:

$$(M_p)_{body_{int}} = 2P'_{ult}\delta_2\delta'_{int} = 54\ kNm$$

$$P_{ult,mod} = 1798.6\ kN$$

7 CONCLUSION

Previous studies on the RSFJ self-centring brace validated that the brace needs strengthening where dampers are located because of the low elastic buckling capacity of the brace. For this purpose, a telescopic mechanism has been put forth to tackle the issue and increase the elastic buckling capacity. Still, there was a need for a proper design procedure to quantify the capacity of the brace in compression as the elastic buckling cannot be a reliable indicator.

This paper presents and proposes a procedure to quantify the ultimate strength of the RSFJ self-centring brace in compression. The procedure starts with calculating the elastic buckling of the system based on which the curve entitled “stiffness degradation path” is derived. Then, the curves entitled “strength degradation path” is derived based on the combined action formulation. The intersection point between these two curves will yield the theoretical upper limit of the ultimate strength. The procedure ends with bringing the upper limit down to calibrated value reflecting the *real* ultimate strength of the system. In this regard, a number of numerical analysis has been done to verify this framework. Furthermore, capacity design considerations are also discussed in the paper.

8 REFERENCE

AISC (2010). AISC 360-10 Specification for Structural Steel Buildings Chicago, IL.

Bagheri, H., A. Hashemi, S. Yousef-beik, P. Zarnani and P. Quenneville (2020). "A new self-centering tension-only brace using resilient slip friction joint: experimental tests and numerical analysis." Journal of Structural Engineering.

Bagheri, H., A. Hashemi, P. Zarnani and P. Quenneville (2020). "The resilient slip friction joint tension-only brace beyond its ultimate level." Journal of Constructional Steel Research 172: 106225.

Bažant, Z. P. and L. Cedolin (2010). Stability of structures: elastic, inelastic, fracture and damage theories, World Scientific.

Darani, F., P. Zarnani, E. Haemmerle, A. Hashemi and P. Quenneville (2018). "Application of new resilient slip friction joint for seismic damage avoidance design of rocking concrete shear walls."

Hashemi, A., H. Bagheri, S. M. M. Yousef-Beik, F. M. Darani, A. Valadbeigi, P. Zarnani and P. Quenneville (2020). "Enhanced Seismic Performance of Timber Structures Using Resilient Connections: Full-Scale Testing and Design Procedure." Journal of Structural Engineering 146(9): 04020180.

Hashemi, A., S. M. M. Yousef-Beik, F. M. Darani, G. C. Clifton, P. Zarnani and P. Quenneville (2019). "Seismic performance of a damage avoidance self-centring brace with collapse prevention mechanism." Journal of Constructional Steel Research 155: 273-285.

Hibbeler, R. C. and T. Kiang (2015). Structural analysis, Pearson Prentice Hall Upper Saddle River.

Riks, E. (1979). "An incremental approach to the solution of snapping and buckling problems." International journal of solids and structures 15(7): 529-551.

Sahami, K., P. Zarnani and P. Quenneville (2020). "Introducing a low damage system incorporating rocking braced frame and resilient slip friction joint as a shear key."

Shabankareh, M., S. Veismoradi, P. Zarnani and P. Quenneville (2020). "Seismic damage avoidance design of moment resisting frames with innovative resilient connection."

Veismoradi, S., P. Quenneville, S. M. M. Yousef-Beik and P. Zarnani (2020). "Seismic retrofitting of RC-frames using Resilient Slip Friction Joint toggle-bracing system."

Veismoradi, S., P. Zarnani and P. Quenneville (2019). Development of self-centring Rotational Slip Friction Joint: a novel damage-free damper with large deflections. Pacific Conference on Earthquake Engineering (PCEE) and New Zealand Society for Earthquake Engineering (NZSEE), Auckland, New Zealand.

Yousef-beik, S. M. M., H. Bagheri, S. Veismoradi, P. Zarnani, A. Hashemi and P. Quenneville (2020). "Seismic performance improvement of conventional timber brace using re-centring friction connection." Structures 26: 958-968.

Yousef-beik, S. M. M., S. Veismoradi, P. Zarnani, A. Hashemi and P. Quenneville (2020). "Eperimental Study On Cyclic Performance Of A Damage-Free Brace With Self-Centering Connection." Journal of Structural Engineering 147(1): 04020299.

Yousef-beik, S. M. M., S. Veismoradi, P. Zarnani and P. Quenneville (2020). "A new self-centering brace with zero secondary stiffness using elastic buckling." Journal of Constructional Steel Research 169: 106035.

Yousef-beik, S. M. M., P. Zarnani, A. Hashemi and P. Quenneville (2019). Lateral Instability of Self-centring Braces: Buckling in loading and Unloading. Pacific Conference on Earthquake Engineering. Auckland, New Zealand.

Zarnani, P. and P. Quenneville (2015). A Resilient Slip Friction Joint. N. I. Office. WO2016185432A1.